ACS Catalysis

Research Article

pubs.acs.org/acscatalysis

# Catalytic Deoxygenation of Octanoic Acid over Supported Palladium: Effects of Particle Size and Alloying with Gold

Keyi Sun,[†] Adria R. Wilson,[‡] Simon T. Thompson,[†] and H. Henry Lamb*[,†]

[†]Department of Chemical and Biomolecular Engineering, North Carolina State University, 911 Partners Way, Raleigh, North Carolina 27695-7905, United States

[‡]Department of Chemistry, Duke University, Box 90354, Durham, North Carolina 27708, United States

**ABSTRACT:** Catalytic deoxygenation of octanoic acid (OA) to *n*-heptane was investigated over silica-supported Pd and PdAu catalysts at 260 °C and 1 atm in a fixed-bed microreactor. $Pd/SiO_2$ catalysts were prepared by incipient wetness (IW) and ion exchange (IE). Bimetallic catalysts were prepared using an IE procedure that is known to produce supported PdAu nanoparticles. The Pd nanoparticles (7.5 nm average size) in the $Pd/SiO_2$ (IW) catalyst exhibit well-defined (100) and (111) facets, as evidenced by high-resolution electron microscopy (HREM) and diffuse reflectance infrared Fourier transform spectroscopy (DRIFTS) of adsorbed CO. As expected, the smaller nanoparticles (1.5 nm average size) in the $Pd/SiO_2$ (IE) catalyst display strong linear and bridging CO DRIFTS bands. The $PdAu/SiO_2$ (1/1 atomic ratio) catalyst contains 5 nm alloy nanoparticles with Pd-rich surfaces, as evidenced by HREM with energy-dispersive X-ray (EDX) analysis and in situ EXAFS spectroscopy. DRIFTS thermal desorption experiments demonstrated that alloying with Au reduced the CO adsorption energy on surface Pd sites. The $Pd/SiO_2$ (IE) catalyst initially exhibited OA decarboxylation and decarbonylation activity but lost decarboxylation activity rapidly with time on stream (TOS). In contrast, the $Pd/SiO_2$ (IW) catalyst had only decarbonylation activity, deactivated less rapidly with TOS, and could be regenerated by heating in $H_2$ to remove OA residues. Alloying Pd with Au was found to improve catalyst stability without significantly affecting decarbonylation activity, as evidenced by the equivalent OA turnover frequencies of the $Pd/SiO_2$ (IW) and $PdAu/SiO_2$ (2/3) catalysts. The geometric and electronic effects of alloying reduce the CO adsorption energy and mitigate self-poisoning by OA and related species.

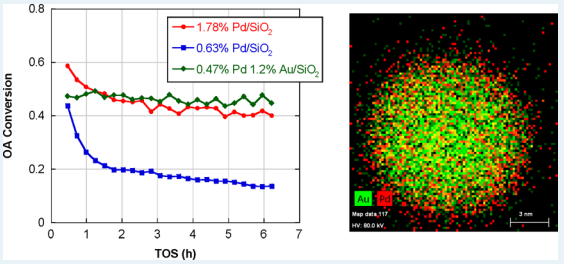


**KEYWORDS:** *fatty acid, decarboxylation, decarbonylation, deactivation, self-poisoning, bimetallic catalyst*

## 1. INTRODUCTION

Bioethanol and biodiesel are widely employed today as substitutes for gasoline and diesel, respectively; however, because of their lower energy densities, poor oxidative stabilities, and incompatibility with engines and transportation fuel infrastructure,[1,2] these first-generation biofuels typically are employed in blends with fossil fuels. Second-generation biofuels that overcome these deficiencies are being developed to provide "drop-in" replacements for conventional petroleum-derived hydrocarbon fuels, including jet fuel. With advances in algae cultivation technology, large areal yields of trigylcerides and fatty acids (FAs) can be produced autotrophically using solar energy.[3] Catalytic deoxygenation can be used to convert FAs to hydrocarbons for transportation fuels via decarboxylation and decarbonylation using supported Pd catalysts.[4−6] These reactions are illustrated below for octanoic acid (OA), the smallest FA found in typical bioderived feedstocks. OA decarboxylation produces *n*-heptane and $CO_2$:

$$C_7H_{15}COOH \rightarrow n\text{-}C_7H_{16} + CO_2 \quad (1)$$

In contrast, OA decarbonylation produces heptene(s), CO and $H_2O$:

$$C_7H_{15}COOH \rightarrow CO + C_7H_{14} + H_2O \quad (2)$$

Typically, the decarboxylation pathway is preferred for biofuel production, because it eliminates the $H_2$ required for alkene hydrogenation and avoids the generation of CO, a noble metal catalyst poison.

Murzin and co-workers have reported extensively on liquid-phase deoxygenation of FAs for biofuel production.[4,5,7−10] Various supported transition metals, including Ni, Ru, Pd, Ir, Os, and Rh on silica, alumina, and activated carbon, were evaluated for semibatch liquid-phase stearic acid (SA) deoxygenation in dodecane.[5] Pd on activated carbon (Pd/C) was identified as highly active and selective for SA decarboxylation to *n*-heptadecane at 300 °C and 17.5 atm under flowing He. Immer and Lamb found that 5 wt % Pd/C deactivated very rapidly under He in fed-batch operation; however, quasi-steady-state SA decarboxylation activity was achieved under 5% $H_2$ with low net $H_2$ consumption.[11] Ford et al. investigated the influence of the support and FA alkyl chain

Received: July 19, 2014
Revised: February 6, 2015
Published: February 10, 2015




DOI: 10.1021/cs501865n
ACS Catal. 2015, 5, 1939−1948

length on initial deoxygenation kinetics using supported Pd catalysts at 300 °C and 15 atm under 5% $H_2$.[12] In comparison to 5 wt % Pd/C, 5 wt % Pd/$SiO_2$ catalysts were less active and exhibited much lower $CO_2$ selectivity. A well-dispersed 5 wt % Pd/$Al_2O_3$ catalyst had high initial SA decarboxylation activity but deactivated rapidly. For even-numbered $C_{10}$−$C_{18}$ FAs, as the carbon number decreased, the reaction completion time increased and $CO_2$ selectivity and initial decarboxylation rate decreased over 5% Pd/C. Simakova et al.[9] reported that a 1 wt % Pd/C catalyst containing 1.7 nm Pd particles had the highest turnover frequency (TOF) ($1.1 \times 10^{-1}$ $s^{-1}$) for deoxygenation of SA−palmitic acid mixtures in the liquid phase (dodecane solvent) at 300 °C and 17.5 atm under 5% $H_2$.

Gas-phase deoxygenation of aliphatic acids (with the exception of acetic acid) over Pd catalysts has been studied less extensively. Early work by Maier et al.[13] showed that Pd/$SiO_2$ was active for gas-phase deoxygenation of OA at 330 °C and 1 atm under flowing $H_2$. OA deoxygenation was assumed to occur via decarboxylation; however, no reaction was observed when an inert $N_2$ carrier gas was employed. Boda et al. studied OA deoxygenation over Pd/C at 360 °C under elevated $H_2$ pressure (10 or 17 atm) in a continuous-flow reactor. OA decarbonylation was proposed to occur via a formic acid intermediate that rapidly decomposes to CO and $H_2O$.[14] Lugo-José et al. reported TOFs of $(5–10) \times 10^{-3}$ $s^{-1}$ for gas-phase deoxygenation of propanoic acid to ethane over Pd/$SiO_2$ catalysts at 200 °C and 1 atm under 20% $H_2$.[15] Alotaibi et al. reported a similar TOF for propanoic acid decarbonylation to ethene over Pd/$SiO_2$ at 250 °C under $H_2$ at 1 atm.[16]

Pd-containing bimetallic catalysts have attracted much attention because of their enhanced performance in comparison to monometallic Pd catalysts.[17] Among the various bimetallics, Pd−Au catalysts have been extensively investigated and employed for many important applications, including vinyl acetate synthesis,[18] low-temperature CO oxidation,[19] and formic acid decomposition.[20] Bimetallic enhancement of catalyst activity, selectivity, and stability may be attributed to geometric (ensemble) and electronic (ligand) effects. Both types of effects have been used to describe the catalytic modification of Pd by Au.[21] Herein, we use PdAu alloys to probe the structure sensitivity of alkyl carboxylic acid deoxygenation over Pd. Previous computational work by Neurock indicated that the activation energy for acetic acid deoxygenation is increased substantially by substituting inert Au atoms for Pd atoms in the active surface ensemble.[22] Our group previously reported X-ray absorption spectroscopy of PdAu/$SiO_2$ catalysts prepared by the method of Lam and Boudart,[23] and consequently, it was a convenient starting point for this work.

In this work, gas-phase deoxygenation of OA to *n*-heptane was investigated over Pd/$SiO_2$ and PdAu/$SiO_2$ catalysts at atmospheric pressure in a fixed-bed microreactor. Pd/$SiO_2$ catalysts prepared by incipient wetness impregnation and ion exchange were used to elucidate particle-size effects on reaction pathways, kinetics, and catalyst deactivation. The monometallic catalysts were characterized by CO chemisorption, diffuse reflectance infrared Fourier transform spectroscopy (DRIFTS), transmission electron microscopy (TEM), and temperature-programmed hydride decomposition (TPHD). PdAu/$SiO_2$ catalysts were prepared using an ion exchange procedure known to produce supported PdAu alloy nanoparticles.[23] In addition to the above techniques, the bimetallic catalysts were characterized by analytical TEM with energy dispersive X-ray (EDX) analysis and in situ extended X-ray absorption fine structure (EXAFS) spectroscopy. Alloying Pd with Au is shown to improve catalyst stability without sacrificing OA deoxygenation activity.

## 2. EXPERIMENTAL METHODS

**2.1. Materials.** OA (98+%) was purchased from Sigma-Aldrich and used as received. Ultrahigh-purity (99.999%) He and $H_2$ were purchased from National Welders. $Pd(NO_3)_2 \cdot xH_2O$ and $[Pd(NH_3)_4][NO_3]_2$ were purchased from Strem Chemicals. $[Au(en)_2]Cl_3$ (en = ethylenediamine) was prepared from $HAuCl_4$ (Sigma-Aldrich), as described in the literature.[24] The silica support was Aerosil 300 from Evonik.

**2.2. Catalyst Preparation.** Pd/$SiO_2$ catalysts were prepared by incipient wetness (IW) impregnation and ion exchange (IE). The Pd/$SiO_2$ (IW) catalysts were prepared by impregnation of silica with an aqueous $Pd(NO_3)_2$ solution of the appropriate volume to form a thick paste. Specifically, $Pd(NO_3)_2 \cdot xH_2O$ was dissolved in 19 mL of deionized (DI) water and added slowly to 4 g of silica. The resultant paste was dried at 40 °C overnight and then calcined at 300 °C in flowing $O_2$ for 2 h. The Pd/$SiO_2$ (IE) catalyst was prepared by contacting the silica support with a dilute aqueous solution of $[Pd(NH_3)_4][NO_3]_2$, as described previously for Pt.[25] After 24 h, the solid was recovered by filtration and washed three times with DI water. The resultant paste was dried at 40 °C overnight and calcined at 250 °C in flowing $O_2$ for 2 h. The bimetallic catalyst PdAu/$SiO_2$ was prepared by ion exchange of $[Pd(NH_3)_4][NO_3]_2$ and $[Au(en)_2]Cl_3$ with silica from a pH 9 slurry.[26] After filtration and washing with DI water, the resultant paste was dried at 100 °C in air overnight, resulting in a purplish brown powder. The Pd and Au loadings were determined by Galbraith Laboratories using inductively coupled plasma−optical emission spectrometry (ICP-OES).

**2.3. Catalyst Characterization.** Pd dispersion was measured by volumetric CO chemisorption using a Micromeritics ASAP 2020c instrument. Prior to chemisorption measurements, the samples were reduced in $H_2$ at 300 °C for 2 h followed by evacuation at 300 °C for 4 h. Two CO adsorption isotherms were recorded at 35 °C: an initial isotherm and another after subsequent evacuation of the sample at 35 °C for 30 min. The Pd dispersion was calculated on the basis of the difference between the two isotherms (representing strongly adsorbed CO). A CO to surface Pd atom stoichiometry of 0.6 was used in dispersion calculations.[27] The equivalent particle diameter ($d$) was calculated from the fractional dispersion ($D$) using the equation[28]

$$d = \frac{1.12}{D} \tag{3}$$

TPHD measurements were performed using a Micromeritics AutoChem II 2920 instrument. The catalyst was heated at 5 °C/min to 300 °C in 5% $H_2$/Ar and held for 1 h. After the temperature was lowered to ∼40 °C in flowing 5% $H_2$/Ar, $H_2$ evolution during a second temperature ramp to 300 °C was monitored using a thermal conductivity detector (TCD).

DRIFT spectra of adsorbed CO were measured using a Bruker Vertex 70 FTIR spectrometer equipped with a Harrick Praying Mantis diffuse-reflectance accessory and a high-temperature in situ DRIFTS cell. Samples were reduced in the cell under flowing $H_2$ at 300 °C for 30 min, purged with He, and then cooled to room temperature under flowing He. For each sample, 1 mL pulses of 5% CO/He were used to


DOI: 10.1021/cs501865n
ACS Catal. 2015, 5, 1939−1948

saturate the catalyst surface until no significant change in the DRIFT spectrum was observed. All spectra consist of 128 scans collected at 4 $cm^{-1}$ resolution using a liquid $N_2$ cooled MCT detector. Thermal desorption experiments were conducted in the DRIFTS cell after CO chemisorption at 25 °C. The catalyst temperature was increased incrementally from 25 to 260 °C under flowing He. After 15 min at each desorption temperature, to avoid thermal artifacts the sample was cooled to 25 °C, and the DRIFT spectrum was recorded.

Conventional transmission electron microscopy (TEM) and high-angle annular dark-field scanning TEM (HAADF-STEM) were used to determine particle size distributions and examine the atomic scale structure of the supported catalysts. Bright-field TEM images were acquired on a FEI Tecnai $G^2$ Twin instrument with 0.3 nm resolution using a 200 kV acceleration voltage (Duke University). HAADF-STEM imaging of the Pd/$SiO_2$ (IW) catalyst was done using a JEOL 2010F microscope operating at 200 kV. An FEI Titan STEM with EDX capability was used to characterize the elemental composition of the PdAu nanoparticles.

Pd K and Au $L_3$ edge X-ray absorption spectroscopy (XAS) of the PdAu/$SiO_2$ (1/1) catalyst was conducted on beamline X-11A of the National Synchrotron Light Source at Brookhaven National Laboratory. The storage ring operated at 2.58 GeV with a current of 150−275 mA. The Si(311) monochromator was calibrated using Au and Pd foils. The monochromator was detuned by 30% at the Au $L_3$ edge to minimize higher harmonics. Measurements were made in transmission mode. For Au $L_3$ edge XAS, the $I_0$ ionization chamber contained flowing $N_2$ and the $I$ chamber contained flowing Ar. For Pd edge XAS, the $I_0$ and $I$ chambers contained flowing Ar. A sample (~250 mg) was pressed into a rectangular slot in a stainless steel sample holder that was then mounted in an in situ XAS cell.[29] The sample was reduced at 300 °C in flowing 5% $H_2$/He for 1 h, purged briefly with He, and cooled in flowing He to 25 °C. Au $L_3$ (three scans) and Pd K (five scans) edge spectra were recorded with the sample under He.

XAS data were processed to isolate EXAFS spectra from the background using Athena software.[30] Replicate scans were averaged to increase the signal-to-noise ratios. The resulting $\chi$ spectra ($k$ space) were Fourier transformed (Pd K, $\Delta k$ = 2.4−12.2 $Å^{-1}$; Au $L_3$, $\Delta k$ = 2.5−12.7 $Å^{-1}$) and fitted in $R$ space (Pd K, $\Delta R$ = 1.4−3.3 Å; Au $L_3$, $\Delta R$ = 1.4−3.4 Å) using Artemis software.[31] Pd−Pd, Pd−Au, Au−Au, and Au−Pd single-scattering paths were generated using FEFF.[32] Amplitude reduction factors, for the Pd−Pd and Au−Au paths, $S_0^2$ = 0.76 and 0.80, respectively, were determined by fitting the EXAFS of Pd and Au foils, respectively. The reported EXAFS parameters $N$ (coordination number), $R$ (interatomic distance), $\sigma^2$ (Debye−Waller factor), and $\Delta E_0$ (inner potential shift) are based on simultaneous fits of $k^n$-weighted spectra ($n$ = 1−3).

**2.4. OA Deoxygenation Experiments.** OA deoxygenation experiments were conducted in a 0.5 in. stainless steel tubular reactor using 0.5 g of catalyst powder suspended between quartz wool plugs. The catalyst temperature was measured using a type K thermocouple in direct contact with the bed. Gas flow rate and composition to the reactor were set by mass flow controllers (Brooks), and OA was fed via high-pressure syringe pump (ISCO Series D) at 4 μL/min (typical flow rate). The standard in situ catalyst pretreatment procedure was heating at 300 °C for 1 h in flowing $H_2$. Typically, the catalyst was brought on stream at 260 °C in flowing 10% $H_2$/He or $H_2$ (100 sccm), and the reaction conditions were maintained for 8−10 h.

The reactor effluent was analyzed using dual online gas chromatographs (GCs). A Shimadzu GC-2010 instrument equipped with a flame ionization detector (FID) was used to measure the reactant and product concentrations in the reactor effluent. Periodic sampling was achieved by using a heated Valco six-port injection valve with a 100 μL sample loop. An Econocap EC-1 capillary column was used, and the GC oven temperature was programmed as follows: 10 °C/min ramp from 70 to 100 °C and then an increase to 240 °C at 40 °C/min. FID responses were calibrated using a series of different concentrations of OA, $n$-heptane, 1-heptene, octanal, 1-octanol, heptanal, and diheptyl ketone in suitable solvents. An SRI GC equipped with a TCD and a Restek ShinCarbon ST 100 column was used for monitoring CO and $CO_2$ concentrations. The GC-TCD was operated isothermally at 100 °C. A standard calibration mixture containing 5% CO, 5% $CO_2$, 5% $H_2$, and 1% $CH_4$ (National Welders) was used to calibrate the GC-TCD for CO, $CO_2$, and $CH_4$ response factors.

OA deoxygenation rates at 260 °C in 10% $H_2$/He were determined from $n$-heptane yields measured under differential conversion conditions. Differential conversion (≤10%) of OA was achieved by increasing the OA injection rate and the feed flow rate of 10% $H_2$/He proportionally to increase the weight hourly space velocity (WHSV) at constant OA concentration. In some instances, it was necessary to reduce the catalyst mass by diluting the bed with inert quartz chips. Small concentrations (<1% each) of impurities and/or thermal reaction products, diheptyl ketone, heptanal, and octanal, were detected by GC-FID in blank (empty tube) experiments with OA (4 μL/min) in 10% $H_2$ at 260 °C. The absence of external and internal diffusional limitations was confirmed using the Mears and Weisz−Prater criteria, respectively.[33]

## 3. RESULTS AND DISCUSSION

**3.1. Characterization of Fresh Catalysts.** ICP-OES and CO chemisorption results for the Pd/$SiO_2$ and PdAu/$SiO_2$ catalysts are given in Table 1. As expected, the Pd/$SiO_2$ (IE) catalyst has a much higher Pd dispersion than the Pd/$SiO_2$ (IW) catalyst. The calculated dispersion of the Pd/$SiO_2$ (IE) catalyst exceeds 100%, indicating that the CO/Pd stoichiometry for these particles is greater than 0.6. Applying a CO/Pd

**Table 1. Catalyst Composition and CO Chemisorption Results**

| catalyst composition | strongly adsorbed CO (μmol/g) | Pd dispersion (%)[a] | particle size (nm) | |
|---|---|---|---|---|
| | | | CO | TEM |
| 1.78% Pd/$SiO_2$ (IW) | 15.7 ± 0.6 (15.0 ± 0.5)[b] | 15.7 (15.0) | 7.1 | 7.5 |
| 0.63% Pd/$SiO_2$ (IE) | 45.9 ± 0.4 (8.0 ± 1.2)[b] | 130 (22.5) | 1.1 | 1.5 |
| 0.44% Pd 0.91% Au/$SiO_2$ (1/1) | 8.2 ± 0.4 | 33.0 | 3.4 | 5.0 |
| 0.42% Pd 1.2% Au/$SiO_2$ (2/3) | 7.8 ± 0.9 | 33.0 | 3.4 | |

[a]Computed using 0.6 CO per surface Pd atom and assuming negligible strongly adsorbed CO on Au. [b]Used catalyst following ex situ reduction at 300 °C in flowing $H_2$.



DOI: 10.1021/cs501865n
ACS Catal. 2015, 5, 1939−1948

stoichiometry of ~0.8, as suggested by Fagherazzi et al.[34] on the basis of small-angle X-ray scattering measurements on 2.0 nm silica-supported Pd particles, would result in a calculated Pd dispersion of 100%. The average particle sizes estimated from CO chemisorption are ~1 and ~7 nm, for the $Pd/SiO_2$ (IE) and $Pd/SiO_2$ (IW) catalysts, respectively. The Pd dispersions of the PdAu bimetallic catalysts are equivalent and lie between those of the Pd monometallic catalysts. The $Pd/SiO_2$ (IE) and $PdAu/SiO_2$ catalysts have comparable Pd loadings but very different surface Pd atom densities. The estimated size of the alloy particles in the $PdAu/SiO_2$ catalysts is ~3.5 nm. However, this estimate assumes negligible irreversible CO adsorption on Au and a uniform Pd distribution in the particles: i.e., no Pd surface enrichment.

TEM images of the $Pd/SiO_2$ (IW), $Pd/SiO_2$ (IE) and $PdAu/SiO_2$ (1/1) catalysts are shown in Figure 1. The $Pd/SiO_2$ (IW)

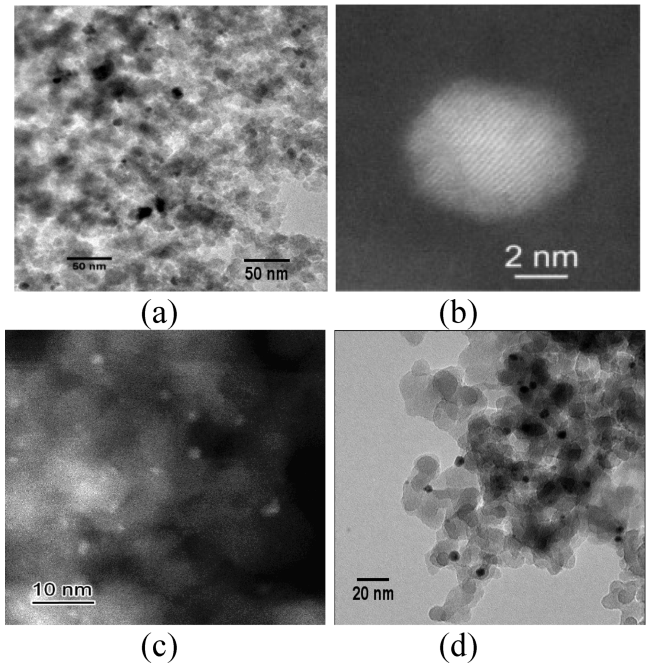


**Figure 1.** TEM images of (a, b) $Pd/SiO_2$ (IW), (c) $Pd/SiO_2$ (IE), and (d) $PdAu/SiO_2$ (1/1) catalysts.

catalyst (Figure 1a) has an average particle size of 7.5 nm with a broad size distribution (Figure 2a) that is skewed toward larger sizes. A dark-field HAADF-STEM image (Figure 1b) illustrates that individual nanoparticles in this catalyst exhibit well-defined low-index facets. The $Pd/SiO_2$ (IE) catalyst contains 1−2 nm Pd particles, seen as bright spots in the dark-field STEM image (Figure 1c). The average particle size is 1.5 nm with a narrow size distribution (Figure 2b). The average particle sizes from TEM agree well with those determined by CO chemisorption for the monometallic catalysts. The nanoparticles in the $PdAu/SiO_2$ (1/1) catalyst (Figure 1d) have a 5 nm average diameter with a relatively broad size distribution (Figure 2c). The average particle size from TEM is significantly larger than that from CO chemisorption, consistent with Pd surface enrichment (at least in the presence of adsorbed CO).[27] The alloy surface composition estimated from the chemisorption data and the TEM average particle size is ~70% Pd. The EDX maps (Figure 3) of an individual nanoparticle from the $PdAu/SiO_2$ (1/1) catalyst provide direct evidence of alloying; however, there are more Pd atoms than Au atoms near the nanoparticle

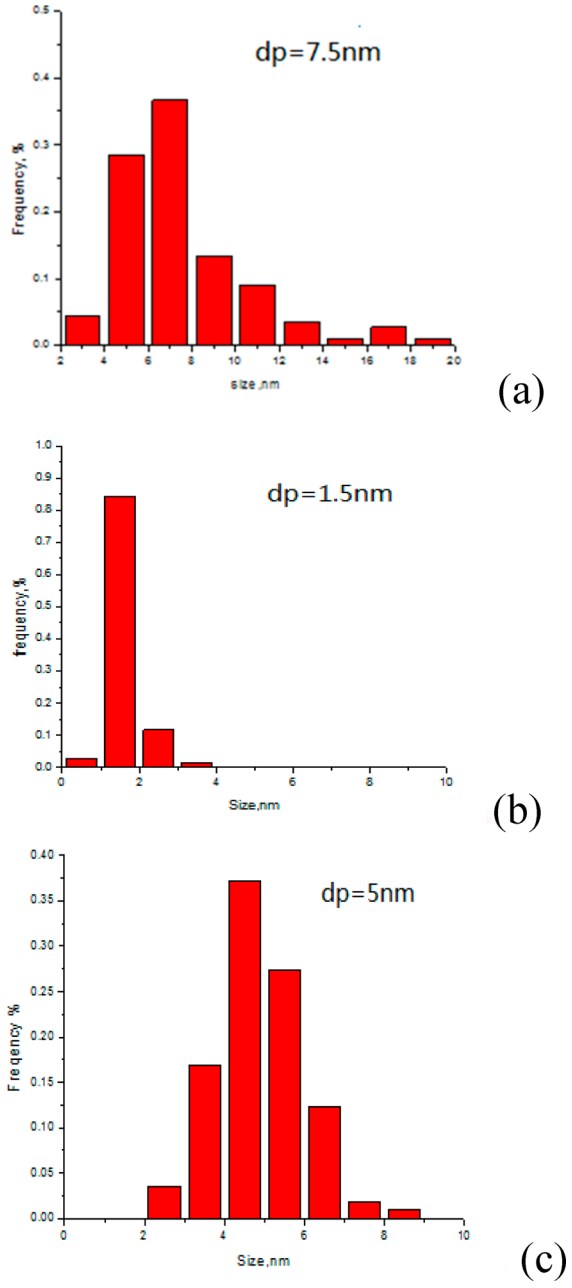


**Figure 2.** TEM particle size distributions of (a) $Pd/SiO_2$ (IW), (b) $Pd/SiO_2$ (IE), and (c) $PdAu/SiO_2$ (1/1) catalysts.

surface (on the basis of the larger diameter in the Pd pixel map). Because the EDX measurements were made ex situ, we could not ascertain if the observed Pd surface enrichment was induced by air exposure.

The $PdAu/SiO_2$ (1/1) catalyst was analyzed by XAS at the Pd K and Au $L_3$ edges. The EXAFS spectra were fit in *R* space using three adjustable parameters for each scattering path: Pd−Au, Pd−Pd, Au−Au, and Au−Pd (where the absorber atom is listed first and the backscatterer second). The inner potential corrections ($\Delta E_0$) for each path for a given absorber were fixed at the values in Table 2. When the Pd K and Au $L_3$ EXAFS spectra were fit independently, the results (Table 2) are in reasonable agreement with those reported by Reifsnyder and Lamb, who analyzed the EXAFS spectra of similarly prepared $PdAu/SiO_2$ catalysts using a combination of empirical and theoretical references.[26] Moreover, the results conform to the


DOI: 10.1021/cs501865n
*ACS Catal.* 2015, 5, 1939−1948

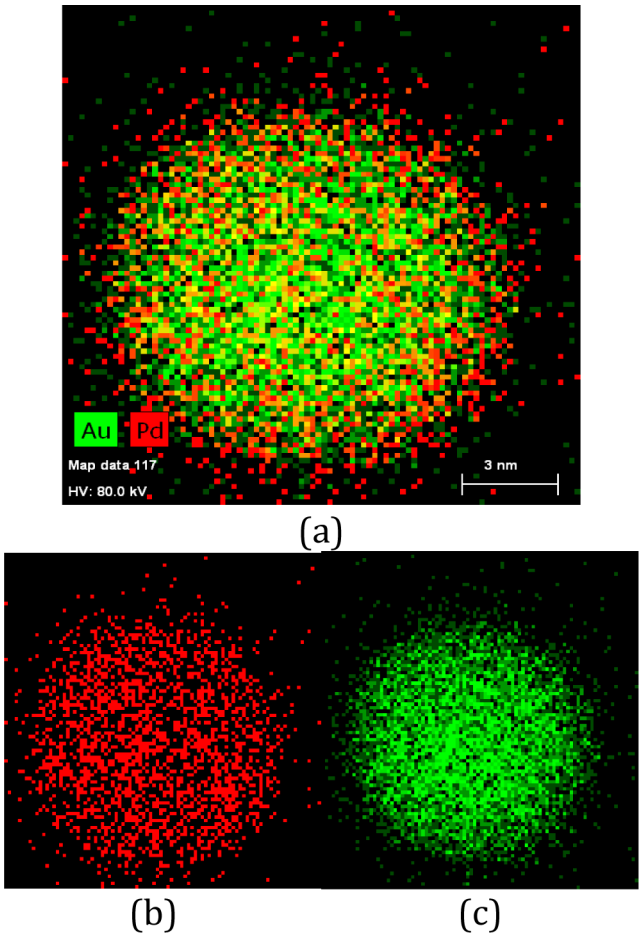


**Figure 3.** STEM-EDX of PdAu nanoparticles from PdAu/$SiO_2$ (1/1) catalyst: (a) Pd–Au composite pixel map, (b) Pd map, and (c) Au map.

consistency criteria originally proposed by Via et al.[35] Strong interference between the EXAFS signals from homometallic and heterometallic scattering paths is apparent in each spectrum (Figure 4). The high-quality fits of the EXAFS spectra illustrated in Figure 4 are confirmed by the small *R* factors in Table 2; an *R* factor of less than 0.05 indicates a good fit. The heterometallic (Pd–Au and Au–Pd) distances are equivalent within experimental uncertainty but shorter than the Vegard's law prediction for a 1/1 PdAu alloy (2.815 Å). The Pd–Pd distance is equivalent to the Pd–Au distance; however, the Au–Au distance is 0.03 Å longer than the Au–Pd distance. The total coordination number for Au (11.1) is greater than that for Pd (8.8), indicating that Pd atoms preferentially occupy surface sites (and conversely, Au atoms are in a more bulklike environment). The larger Au–Au coordination number (relative to Au–Pd) and longer Au–Au distance evidence that the supported alloy nanoparticles have Au-rich cores. Thus, the Pd surface enrichment indicated by CO chemisorption and EDX analysis is confirmed by in situ EXAFS spectroscopy.

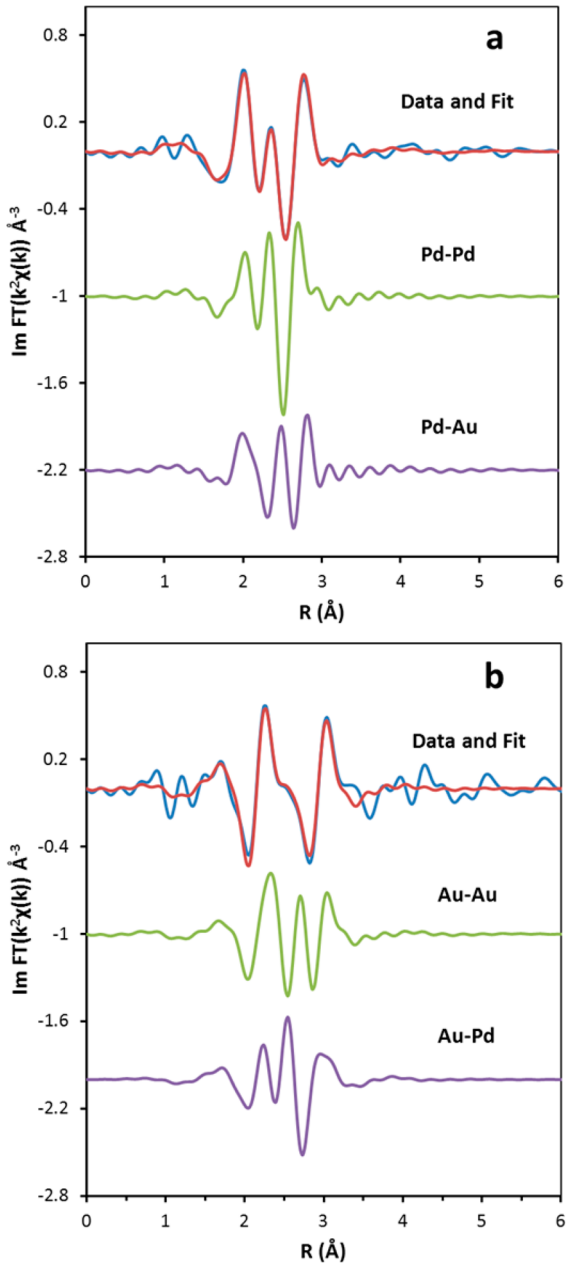


**Figure 4.** Pd K (a) and Au $L_3$ (b) EXAFS data and fits for PdAu/$SiO_2$ (1/1) catalyst showing the imaginary part of the $k^2$-weighted Fourier transforms. Individual components of the fits are shown offset below.

Bulk hydride formation and decomposition have been used to assess the degree of alloying in Pd-containing bimetallic catalysts.[36,37] For relatively large supported Pd particles (~10 nm) previously saturated with hydrogen, a *β*-Pd hydride decomposition peak is observed at 70–90 °C in flowing 10% $H_2$.[37,38] For smaller Pd particles, the higher surface-to-volume results in a lower H/Pd ratio[39] and a lower hydride

**Table 2. EXAFS Spectroscopy Results for PdAu/$SiO_2$ (1/1) Catalyst**

| absorber | backscatterer | *N* | *R* (Å) | $\sigma^2$ ($10^{-3}$Å$^2$) | $\Delta E_0$ (eV) | *R* factor |
|---|---|---|---|---|---|---|
| Pd | Pd | 4.2 ± 0.6 | 2.79 ± 0.01 | 7.7 ± 1.2 | −6 | 0.02 |
| | Au | 4.6 ± 0.6 | 2.79 ± 0.01 | 8.0 ± 1.0 | −6 | |
| Au | Au | 7.0 ± 1.2 | 2.83 ± 0.01 | 8.1 ± 1.3 | 3 | 0.03 |
| | Pd | 4.1 ± 0.9 | 2.80 ± 0.01 | 8.7 ± 1.5 | 3 | |



DOI: 10.1021/cs501865n
*ACS Catal.* 2015, 5, 1939–1948

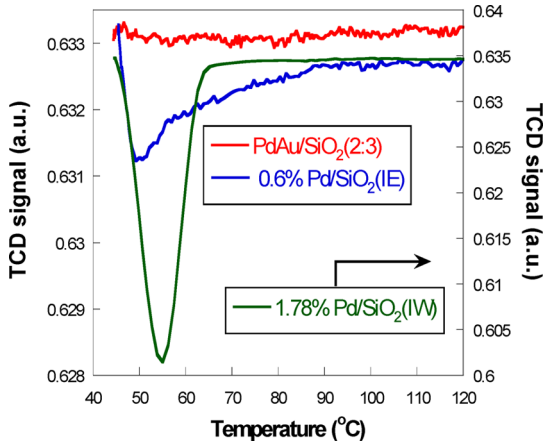


**Figure 5.** TPHD profiles of $Pd/SiO_2$ (IW), $PdSiO_2$ (IE), and $PdAu/SiO_2$ (2/3) catalysts.

decomposition temperature.[40,41] For PdAu alloys containing 50 atom % Au or more, the $\beta$-Pd hydride peak is greatly diminished (or completely absent) due to the effects of alloying on bulk electronic structure.[36,42] As shown in Figure 5, the $Pd/SiO_2$ (IW) catalyst exhibits an intense well-defined TPHD peak at 55 °C in flowing 5% $H_2$/Ar. The measured H/Pd ratio (0.65) agrees well with the H/Pd ratio for bulk $\beta$-Pd hydride.[39,42] The $Pd/SiO_2$ (IE) catalyst displays a much smaller TPHD peak at 50 °C that is broad and skewed toward higher temperatures. The measured H/Pd ratio (0.16) is consistent with highly dispersed supported Pd particles.[39,41,43] The TPHD spectrum of $PdAu/SiO_2$ (1/1) does not contain any $\beta$-Pd hydride decomposition features, indicating the absence of segregated Pd particles in this catalyst. Apparently, the combination of relatively small particle size (5 nm) and alloying with Au is sufficient to completely suppress bulk hydride formation.

CO DRIFTS was used to probe the adsorption sites of the $Pd/SiO_2$ and $PdAu/SiO_2$ catalysts. The spectra of the $Pd/SiO_2$ catalysts (Figure 6) exhibit CO stretching bands in the 2000–2100 and 1800–2000 $cm^{-1}$ regions corresponding to linear (atop) and bridging (multicoordinated) CO species, respectively.[44] The DRIFT spectrum of the $Pd/SiO_2$ (IW) catalyst (Figure 6a) contains a strong twofold bridging CO peak at 1990 $cm^{-1}$ and a weak linear CO peak at ~2090 $cm^{-1}$. When this spectrum is considered with the HAADF-STEM image in Figure 1b, it establishes that the $Pd/SiO_2$ (IW) catalyst contains supported Pd nanoparticles with well-defined (100) and (111) facets.[45,46] The unusually sharp and narrow band at 1990 $cm^{-1}$ in Figure 6a may be assigned to CO adsorbed on (100) facets and CO bridge bonded to particle steps and edges, with significant "intensity borrowing" from bridging CO on (111) facets, as discussed in Lear et al. and references therein.[46] The CO DRIFT spectrum of our $Pd/SiO_2$ (IW) catalyst is remarkably similar to that of a 7.3 wt % $Pd/Al_2O_3$ catalyst prepared from tetraamminepalladium(II) tetraazide (Figure 4 of ref 46). In contrast, the $Pd/SiO_2$ (IE) catalyst exhibits strong linear and twofold bridging CO peaks at 2100 and 1930 $cm^{-1}$, respectively (Figure 6b). Previous research has shown that small supported Pd particles have a higher fraction of edge and corner sites that accommodate atop CO species.[47] Moreover, the twofold bridging CO peak shifts to lower frequency because the ratio of (111) to (100) facets increases with decreasing particle size.[48,49]

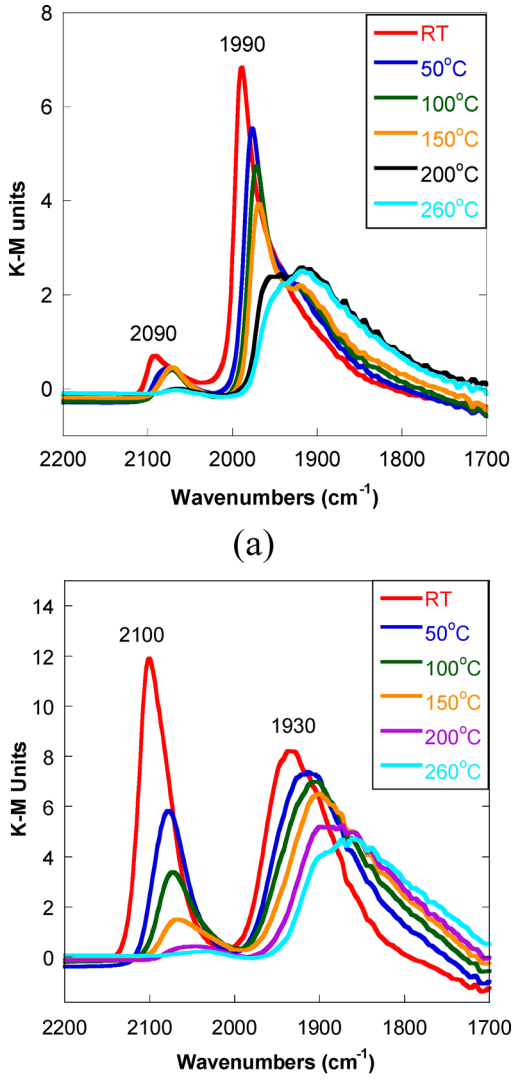


**Figure 6.** CO DRIFT spectra of (a) $Pd/SiO_2$ (IW) and (b) $Pd/SiO_2$ (IE) catalysts. Thermal desorption temperatures (in flowing He) are indicated in the legends.

DRIFT spectra of the $PdAu/SiO_2$ catalysts (Figure 7) exhibit two strong peaks at 2070 and 1960 $cm^{-1}$ that are assigned to linear and 2-fold bridging CO species; however, these features are much less intense than those of the $Pd/SiO_2$ catalysts because of the lower surface Pd atom densities. A shoulder at 2105 $cm^{-1}$ in Figure 7a is assigned to linearly adsorbed CO atop Au atoms,[50] and its intensity increases with Au content (Figure 7b). In addition, the linear-to-bridging intensity ratio increases,[23,51] and the CO peaks narrow with increasing Au content. The $\nu_{CO}$ value of atop CO on Pd sites at saturation coverage is shifted downward by ~30 $cm^{-1}$ relative to atop CO on 1 nm Pd particles. Goodman and co-workers assigned peaks at 2060–2085 $cm^{-1}$ to atop CO on isolated Pd sites of PdAu alloy films and AuPd (100) single crystals.[52] The $\nu_{CO}$ value of the 2-fold bridging species lies between those assigned to bridging CO on Pd(100) and Pd(111) surfaces at saturation coverage and indicates the presence of vicinal Pd atoms on the alloy surface.[27] Goodman and co-workers assigned a peak at 1958 $cm^{-1}$ to CO adsorbed on contiguous Pd surface sites of an ion-sputtered PdAu (100) single crystal. A band at


DOI: 10.1021/cs501865n
ACS Catal. 2015, 5, 1939–1948

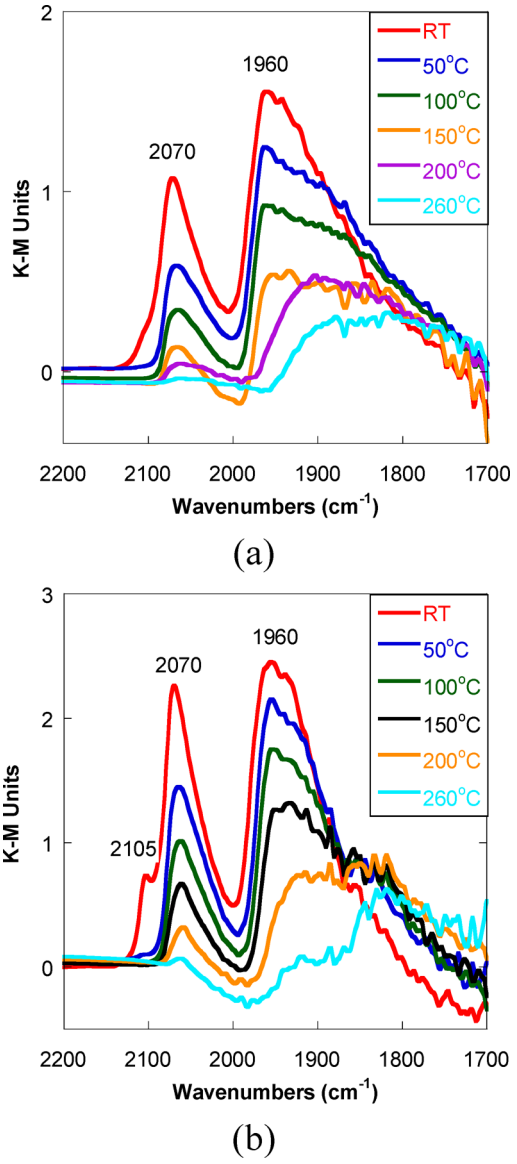


**Figure 7.** CO DRIFT spectra of (a) PdAu/$SiO_2$ (1/1) and (b) PdAu/$SiO_2$ (2/3) catalysts. Thermal desorption temperatures (in flowing He) indicated in the legends.

~1970 $cm^{-1}$ was assigned to CO on contiguous Pd sites created by CO-induced segregation of Pd atoms to the surface.[52]

To assess CO adsorption energies, stepwise thermal desorption experiments were conducted in flowing He beginning with catalysts saturated with CO at 25 °C. As illustrated by the CO DRIFT spectrum of Pd/$SiO_2$ (IE), linear CO desorbs at lower temperatures more completely than bridging CO, indicating a lower heat of adsorption (adsorption energy). Concomitant with CO desorption (reducing surface coverage), the linear and bridging peaks shift to lower wavenumbers, consistent with a reduction in dipolar coupling between adjacent adsorbed CO molecules.[53] Qualitatively similar thermal desorption behavior is shown for the Pd/$SiO_2$ (IW) catalyst in Figure 6a. For both monometallic catalysts, a significant fraction of the adsorbed CO remains in bridging sites after thermal desorption at 260 °C. Moreover, the position and broad shape of the band after 260 °C desorption indicates a mixture of CO in twofold and threefold bridging sites. The thermal desorption behavior of the PdAu/$SiO_2$ catalysts (Figure 7) is different in several aspects. The atop and twofold bridging CO peak positions do not shift appreciably during thermal desorption. In addition, the fractional surface coverage by bridging CO after thermal desorption at 260 °C is less than that for the monometallic samples, especially for the PdAu/$SiO_2$ (2/3) catalyst. These observations are consistent with the expected geometric and electronic effects of alloying Pd with Au. Alloying creates Pd surface ensembles that are diluted by Au and, consequently, are less affected by dipolar coupling. Moreover, alloying with Au weakens the interaction between CO and surface Pd atoms, consistent with electron transfer from Au to the Pd d band.[21,54,55]

**3.2. OA Deoxygenation Catalysis.** The supported Pd catalysts were evaluated for OA deoxygenation under 10% and 100% $H_2$ at 260 °C and 1 atm. Under 10% $H_2$, the Pd/$SiO_2$ (IW) catalyst gave an initial OA conversion of ~55% and deactivated to a stable conversion of ~40% after 4–5 h time on stream (TOS) (Figure 8). Selectivity to *n*-heptane was >93%;

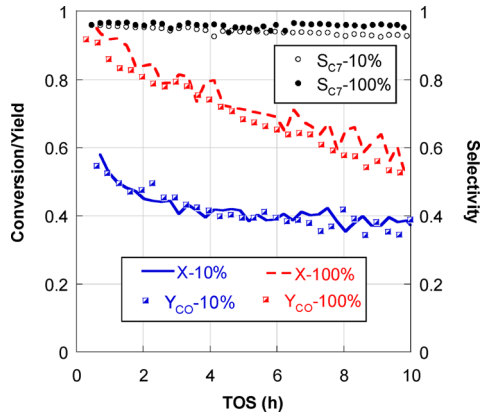


**Figure 8.** Catalytic deoxygenation of OA over Pd/$SiO_2$ (IW) catalyst at 260 °C and 1 atm under 10% and 100% $H_2$.

minor products included octanal, 1-octanol, and heptanal. CO yield and OA conversion with TOS agree closely, indicating that decarbonylation is the dominant reaction pathway. The *n*-heptane product may result either from rapid hydrogenation of heptene(s) formed via eq 2 or from decarbonylation of octanal resulting from OA hydrogenation.[56] The water-gas shift (WGS) reaction, in principle, can disguise the deoxygenation pathway; however, the equilibrium constant for WGS is 71.4 at 260 °C.[57] Under 10% $H_2$, the equilibrium $CO_2$ selectivity in our OA deoxygenation experiments would be approximately 50%; however, $CO_2$ was not detected as a product, indicating negligible WGS activity for this catalyst.

Under 100% $H_2$, initial OA conversion was ~100% (Figure 8); however, the catalyst deactivation rate was significantly higher, and stable activity was not achieved even after >8 h TOS. In this case, the CO yield with TOS was ~3% lower than OA conversion; selectivity to *n*-heptane was >95%. Higher $H_2$ partial pressure should favor OA hydrogenation to octanal that subsequently undergoes decarbonylation to *n*-heptane.[56] The rapid deactivation of the Pd/$SiO_2$ (IW) catalyst under 100% $H_2$ may be related to its increased decarbonylation activity. Endogenous CO will block active sites if it is not desorbed completely (irreversibly) under reaction conditions.[11] As evidenced by DRIFTS, CO does not desorb completely from this catalyst at 260 °C in flowing He, and CO poisoning may be responsible for the observed catalyst deactivation.


DOI: 10.1021/cs501865n
*ACS Catal.* 2015, 5, 1939–1948

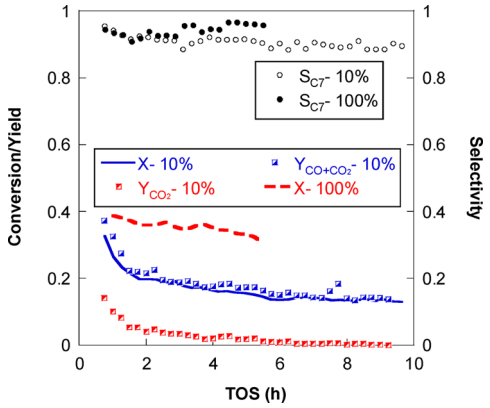


**Figure 9.** Catalytic deoxygenation of OA over $Pd/SiO_2$ (IE) catalyst at 260 °C and 1 atm under 10% and 100% $H_2$.

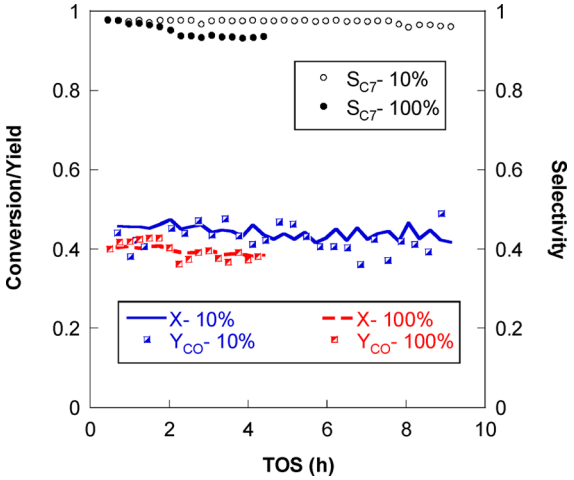


**Figure 10.** Catalytic deoxygenation of OA over $PdAu/SiO_2$ (2/3) catalyst at 260 °C and 1 atm under 10% and 100% $H_2$.

OA deoxygenation results for the $Pd/SiO_2$ (IE) catalyst are shown in Figure 9. Initial deoxygenation activity was lower than that for the $Pd/SiO_2$ (IW) catalyst despite the more than twofold greater surface Pd atom density. Under 10% $H_2$, $Pd/SiO_2$ (IE) gave an initial OA conversion of 35−40% and exhibited both decarbonylation and decarboxylation activity; however, the initial decarboxylation activity (as measured by $CO_2$ yield) decayed to essentially zero after 5 h TOS. Good agreement is observed between the *n*-heptane yield and the CO + $CO_2$ yield (Figure 9), demonstrating closure of the material balance. After 5 h TOS, the catalyst approached a stable conversion of ∼15% with 90% *n*-heptane selectivity. Octanal, heptanal, and diheptyl ketone were minor products. Diheptyl ketone was detected only at low conversions (<20%), and it represented <1% of the reaction products. The $Pd/SiO_2$ (IE) catalyst exhibited similar initial activity under 100% $H_2$ (Figure 9). Unfortunately, temporal GC-TCD data are not available for this experiment; however, it seems safe to assume that CO was the main $C_1$ product under these conditions. Selectivity to *n*-heptane was 90−95%. In contrast to the $Pd/SiO_2$ (IW) catalyst, the $Pd/SiO_2$ (IE) catalyst deactivated more slowly with TOS under 100% $H_2$. In this case, the higher $H_2$ partial pressure may be more effective at preventing self-poisoning by strongly adsorbed (i.e., fully or partially dehydrogenated) intermediates on the small 1−2 nm Pd particles or inhibiting polymerization of heptenes. Theoretical

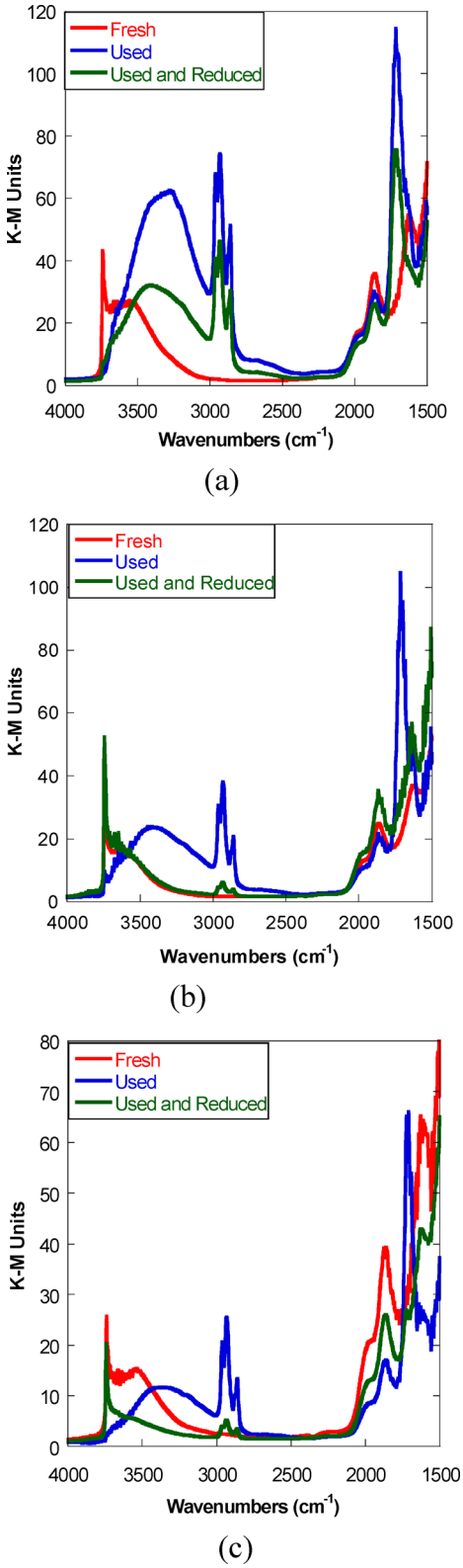


**Figure 11.** DRIFT spectra of (a) $Pd/SiO_2$ (IE), (b) $Pd/SiO_2$ (IW), and (c) $PdAu/SiO_2$ (2/3) catalysts: fresh, used, and used after treatment in flowing $H_2$ at 300 °C.

investigations of the deoxygenation of propanoic and butanoic acids on Pd(111) have revealed the importance of dehydrogenated surface intermediates in the decarboxylation and decarbonylation pathways.[58,59]



DOI: 10.1021/cs501865n
*ACS Catal.* 2015, 5, 1939−1948

Table 3. TOF Values for Deoxygenation of Alkyl Carboxylic Acids over $Pd/SiO_2$

| catalyst | acid | $T$ (°C) | $H_2$ (%) | $P$ (atm) | TOF ($10^{-3}$ $s^{-1}$) | ref |
|---|---|---|---|---|---|---|
| 1.1 wt % $Pd/SiO_2$ | propanoic | 200 | 20 | 1 | 11 | 15 |
| 4.0 wt % $Pd/SiO_2$ | propanoic | 200 | 20 | 1 | 5.3 | 15 |
| 0.5 wt % $Pd/SiO_2$ | propanoic | 250 | 100 | 1 | 9.4 | 16 |
| 1.78 wt % $Pd/SiO_2$ | octanoic | 260 | 10 | 1 | 41 ± 2.3 | this work |
| 0.42 wt % Pd 1.2 wt % $Au/SiO_2$ | octanoic | 260 | 10 | 1 | 43 ± 3.7 | this work |

Under 10% $H_2$, the $PdAu/SiO_2$ (2/3) catalyst achieved an initial OA conversion of ∼45% despite its lower Pd surface atom density, and it did not deactivate significantly with TOS (Figure 10). Stable OA conversion was sustained for more than 8 h with >97% selectivity to *n*-heptane. CO was the only $C_1$ product. The performance of the $PdAu/SiO_2$ (1/1) catalyst was closely similar under these reaction conditions. Under 100% $H_2$, the $PdAu/SiO_2$ (2/3) catalyst had modestly lower activity and selectivity to *n*-heptane. Several minor products, including octanal, 1-octanol, and diheptyl ketone, were favored under 100% $H_2$. A 1.9 wt % $Au/SiO_2$ catalyst was prepared by depositing 4.3 nm colloidal Au particles onto Aerosil 300, as described by Wilson et al.[60] After calcination at 300 °C in air and in situ reduction at 300 °C in $H_2$, the $Au/SiO_2$ catalyst had no appreciable activity for OA deoxygenation at 260 °C (4 μL/min under 10% $H_2$). OA conversion was less than 5%, and the major products are consistent with either silica-catalyzed reactions (diheptyl ketone) or thermal decomposition. As the $PdAu/SiO_2$ catalysts have much lower Pd loadings (and Pd surface atom densities) than the $Pd/SiO_2$ catalysts, clearly, alloying Pd with Au improves catalyst performance. The improved stability may result from a decrease in CO adsorption energy. The order of residual CO coverage at 260 °C (determined from DRIFTS) is as follows: $Pd/SiO_2$ (IE) ≈ $PdSiO_2$ (IW) > $PdAu/SiO_2$ (1/1) > $PdAu/SiO_2$ (2/3), and this order correlates well with catalyst deactivation behavior. Under 100% $H_2$, the $PdAu/SiO_2$ (2/3) catalyst (Figure 10) had modestly lower activity (40% OA conversion) and *n*-heptane selectivity (>93%); however, the activity declined only very slowly with TOS.

**3.3. Characterization of Used Catalysts.** The dispersion of the used $Pd/SiO_2$ (IW) catalyst after postreaction treatment in $H_2$ at 300 °C is equivalent to that of the fresh catalyst (Table 1). In contrast, chemisorption measurements on the used $Pd/SiO_2$ (IE) catalyst (after an equivalent postreaction treatment) indicate a ∼70−80% decrease in dispersion. TEM imaging of the used $Pd/SiO_2$ (IE) catalyst did not evidence particle sintering under reaction conditions, leading to the inference that irreversibly adsorbed OA (or other organic residues) is responsible for loss of Pd active sites.[61]

DRIFT spectra of the used catalysts (Figure 11) contain new features that are assigned to adsorbed OA species. The spectra of the used catalysts display peaks near 2900 and 1700 $cm^{-1}$ that may be assigned to alkyl C−H and C═O stretching frequencies, respectively. The observed peaks are consistent with the IR spectrum of OA;[62] however, the C═O stretching frequency is red-shifted by ∼65 $cm^{-1}$ relative to gas-phase OA, consistent with either liquid-phase or adsorbed OA. Subsequently, the used catalysts were treated in flowing $H_2$ at 300 °C for 1 h and then purged with He. As shown in Figure 11, OA was removed from the $Pd/SiO_2$ (IW) and $PdAu/SiO_2$ (2/3) catalysts but remained on the $Pd/SiO_2$ (IE) catalyst. Thus, DRIFTS analysis indicates that OA is adsorbed more strongly on the $Pd/SiO_2$ (IE) catalyst that contains smaller (1−2 nm) Pd nanoparticles.

**3.4. TOF Measurements.** Specific rates of OA decarbonylation over the $Pd/SiO_2$ (IW) and $PdAu/SiO_2$ (2/3) catalysts were measured at differential conversion by increasing WHSV at constant OA concentration. Steady-state TOFs were calculated using the measured rates and the surface Pd atom densities of the fresh catalysts from CO chemisorption. The TOFs for gas-phase OA deoxygenation over $Pd/SiO_2$ (IW) and $PdAu/SiO_2$ (2/3) under 10% $H_2$ at 260 °C and 1 atm are $4.1 \times 10^{-2}$ and $4.3 \times 10^{-2}$ $s^{-1}$, respectively. The equivalence of these TOFs suggests that OA decarbonylation requires only a relatively small ensemble of Pd atoms. These TOFs are compared in Table 3 to previously reported values for deoxygenation of aliphatic carboxylic acids in the gas phase over $Pd/SiO_2$ catalysts. Meaningful comparisons are difficult, owing to the range of reaction conditions employed. The reported TOFs for gas-phase deoxygenation of propanoic acid to ethane and propionaldehyde over $Pd/SiO_2$ catalysts are nearly 1 order of magnitude lower than our OA results; however, the reaction conditions are not directly comparable (lower temperature and higher $H_2$ partial pressure).[15,16] A similarly low TOF was reported for propanoic acid decarbonylation over 0.5 wt % $Pd/SiO_2$ at 250 °C in $H_2$; however, the product was ethene, not ethane. The higher TOFs for OA (in comparison to propanoic acid) may be explained (at least in part) by its longer alkyl chain.[12]

## 4. CONCLUSIONS

$Pd/SiO_2$ catalysts are active and highly selective for OA decarbonylation to *n*-heptane at 260 °C under $H_2$; however, they deactivate significantly with TOS, and the deactivation behavior is related to Pd particle size. A highly dispersed $Pd/SiO_2$ catalyst containing 1−2 nm Pd particles deactivates rapidly and irreversibly under 10% $H_2$, apparently due to self-poisoning by OA and strongly adsorbed (i.e., fully or partially dehydrogenated) intermediates. TEM images of the used catalyst show negligible change in Pd particle size, ruling out sintering as a key reason for deactivation. Moreover, this catalyst deactivates much more slowly under 100% $H_2$, suggesting that hydrogen may inhibit the accumulation of unsaturated species on the catalyst surface. A $Pd/SiO_2$ catalyst containing much larger Pd nanoparticles deactivates less rapidly with TOS in 10% $H_2$ and can be regenerated by heating in $H_2$ to remove OA residues. Higher $H_2$ partial pressure substantially increases the initial decarbonylation rate, but this catalyst deactivates more rapidly under 100% $H_2$, apparently due to CO poisoning. Alloying Pd with Au was found to improve catalyst stability without significantly affecting decarbonylation activity. Thermal desorption experiments demonstrate a reduction in the CO adsorption energy on Pd surface sites of the alloy nanoparticles. The equivalence of OA TOFs over $Pd/SiO_2$ (IW) and $PdAu/SiO_2$ (2/3) suggests that decarbonylation requires only a relatively small ensemble of Pd atoms.


DOI: 10.1021/cs501865n
ACS Catal. 2015, 5, 1939−1948

## AUTHOR INFORMATION


### Corresponding Author

*E-mail for H.H.L.: lamb@ncsu.edu.


### Notes

The authors declare no competing financial interest.

## ACKNOWLEDGMENTS

This work was supported by the National Science Foundation under an EFRI HyBi grant (EFRI-0937721). X-ray absorption measurements were conducted using beamline X-11A of the National Synchrotron Light Source at Brookhaven National Laboratory. The authors gratefully acknowledge the assistance of Dr. Xianqin Wang (New Jersey Institute of Technology).

## REFERENCES


(1) Smith, B.; Greenwell, H. C.; Whiting, A. *Energy Environ. Sci.* **2009**, *2*, 262−271.
(2) Knothe, G. *Fuel Process. Technol.* **2005**, *86*, 1059−1070.
(3) Chisti, Y. *Biotechnol. Adv.* **2007**, *25*, 294−306.
(4) Kubičková, I.; Snåre, M.; Eränen, K.; Mäki-Arvela, P.; Murzin, D. Y. *Catal. Today* **2005**, *106*, 197−200.
(5) Snåre, M.; Kubičková, I.; Mäki-Arvela, P.; Eränen, K.; Murzin, D. Y. *Ind. Eng. Chem. Res.* **2006**, *45*, 5708−5715.
(6) Immer, J. G.; Kelly, M. J.; Lamb, H. H. *Appl. Catal., A* **2010**, *375*, 134−139.
(7) Mäki-Arvela, P.; Kubickova, I.; Snåre, M.; Eränen, K.; Murzin, D. Y. *Energy Fuels* **2007**, *21*, 30−41.
(8) Snåre, M.; Kubičková, I.; Mäki-Arvela, P.; Chichova, D.; Eränen, K.; Murzin, D. Y. *Fuel* **2008**, *87*, 933−945.
(9) Simakova, I.; Simakova, O.; Mäki-Arvela, P.; Simakov, A.; Estrada, M.; Murzin, D. Y. *Appl. Catal., A* **2009**, *355*, 100−108.
(10) Lestari, S.; Mäki-Arvela, P.; Bernas, H.; Simakova, O.; Sjöholm, R.; Beltramini, J.; Lu, G. M.; Myllyoja, J.; Simakova, I.; Murzin, D. Y. *Energy Fuels* **2009**, *23*, 3842−3845.
(11) Immer, J. G.; Lamb, H. H. *Energy Fuels* **2010**, *24*, 5291−5299.
(12) Ford, J. P.; Immer, J. G.; Lamb, H. H. *Top. Catal.* **2012**, *55*, 175−184.
(13) Maier, W. F.; Roth, W.; Thies, I.; Schleyer, P. V. R. *Chem. Ber.* **1982**, *115*, 808−812.
(14) Boda, L.; Onyestyák, G.; Solt, H.; Lónyi, F.; Valyon, J.; Thernesz, A. *Appl. Catal., A* **2010**, *374*, 158−169.
(15) Lugo-José, Y. K.; Monnier, J. R.; Williams, C. T. *Appl. Catal., A* **2014**, *469*, 410−418.
(16) Alotaibi, M. A.; Kozhevnikova, E. F.; Kozhevnikov, I. V. *Appl. Catal., A* **2012**, *447*, 32−40.
(17) Coq, B.; Figueras, F. *J. Mol. Catal. A* **2001**, *173*, 117−134.
(18) Han, Y. F.; Wang, J. H.; Kumar, D.; Yan, Z.; Goodman, D. *J. Catal.* **2005**, *232*, 467−475.
(19) Xu, J.; White, T.; Li, P.; He, C.; Yu, J.; Yuan, W.; Han, Y. F. *J. Am. Chem. Soc.* **2010**, *132*, 10398−10406.
(20) Huang, Y.; Zhou, X.; Yin, M.; Liu, C.; Xing, W. *Chem. Mater.* **2010**, *22*, 5122−5128.
(21) Gao, F.; Goodman, D. W. *Chem. Soc. Rev.* **2012**, *41*, 8009−8020.
(22) Neurock, M. Forment, G. F.; Waugh, K. *Dynamics of Surfaces and Reaction Kinetics in Heterogeneous Catalysis*; Elsevier: Amsterdam, 1997; pp 23−24.
(23) Lam, Y.; Boudart, M. *J. Catal.* **1977**, *50*, 530−540.
(24) Block, B.; Bailar, J. C., Jr *J. Am. Chem. Soc.* **1951**, *73*, 4722−4725.
(25) Reifsnyder, S. N.; Otten, M. M.; Sayers, D. E.; Lamb, H. H. *J. Phys. Chem. B* **1997**, *101*, 4972−4977.
(26) Reifsnyder, S. N.; Lamb, H. H. *J. Phys. Chem. B* **1999**, *103*, 321−329.
(27) Kunz, S.; Iglesia, E. *J. Phys. Chem. C* **2014**, *118*, 7468−7479.
(28) Xu, X.; Szanyi, J.; Xu, Q.; Goodman, D. W. *Catal. Today* **1994**, *21*, 57−69.
(29) Kampers, F.; Maas, T.; Van Grondelle, J.; Brinkgreve, P.; Koningsberger, D. *Rev. Sci. Instrum.* **1989**, *60*, 2635−2638.
(30) Ravel, B.; Newville, M. *J. Synchrotron Radiat.* **2005**, *12*, 537−541.
(31) Newville, M. *J. Synchrotron Radiat.* **2001**, *8*, 322−324.
(32) Rehr, J. J.; Albers, R. *Rev. Mod. Phys.* **2000**, *72*, 621.
(33) Fogler, H. S. *Elements of Chemical Reaction Engineering*, 3rd ed,; Prentice Hall: Upper Saddle River, NJ, 1999; p 761.
(34) Fagherazzi, G.; Benedetti, A.; Polizzi, S.; Di Mario, A.; Pinna, F.; Signoretto, M.; Pernicone, N. *Catal. Lett.* **1995**, *32*, 293−303.
(35) Via, G.; Drake, K., Jr.; Meitzner, G.; Lytle, F.; Sinfelt, J. *Catal. Lett.* **1990**, *5*, 25−33.
(36) Ziemecki, S.; Michel, J.; Jones, G. *React. Solid.* **1986**, *2*, 187−202.
(37) Bonarowska, M.; Pielaszek, J.; Juszczyk, W.; Karpiński, Z. *J. Catal.* **2000**, *195*, 304−315.
(38) Chang, T. C.; Chen, J. J.; Yeh, C. T. *J. Catal.* **1985**, *96*, 51−57.
(39) Boudart, M.; Hwang, H. *J. Catal.* **1975**, *39*, 44−52.
(40) Pinna, F.; Signoretto, M.; Strukul, G.; Polizzi, S.; Pernicone, N. *React. Kinet. Catal. Lett.* **1997**, *60*, 9−13.
(41) Nag, N. K. *J. Phys. Chem. B* **2001**, *105*, 5945−5949.
(42) Luo, S.; Wang, D.; Flanagan, T. B. *J. Phys. Chem. B* **2010**, *114*, 6117−6125.
(43) Bonivardi, A. L.; Baltanás, M. A. *J. Catal.* **1992**, *138*, 500−517.
(44) Bradshaw, A.; Hoffmann, F. *Surf. Sci.* **1978**, *72*, 513−535.
(45) Kelly, M. J.; Kim, J.; Roberts, G. W.; Lamb, H. H. *Top. Catal.* **2008**, *49*, 178−186.
(46) Lear, T.; Marshall, R.; Lopez-Sanchez, J. A.; Jackson, S. D.; Klapötke, T. M.; Bäumer, M.; Rupprechter, G.; Freund, H. J.; Lennon, D. *J. Chem. Phys.* **2005**, *123*, 174706.
(47) Giorgi, J. B.; Schroeder, T.; Bäumer, M.; Freund, H. J. *Surf. Sci.* **2002**, *498*, L71−L77.
(48) Szanyi, J.; Kuhn, W. K.; Goodman, D. W. *J. Vac. Sci. Technol. A* **1993**, *11*, 1969−1974.
(49) Rieck, J. S.; Bell, A. T. *J. Catal.* **1987**, *103*, 46−54.
(50) Yi, C. W.; Luo, K.; Wei, T.; Goodman, D. *J. Phys. Chem. B* **2005**, *109*, 18535−18540.
(51) Kugler, E.; Boudart, M. *J. Catal.* **1979**, *59*, 201−210.
(52) Gao, F.; Wang, Y.; Goodman, D. W. *J. Phys. Chem. C* **2009**, *113*, 14993−15000.
(53) Matolin, V.; Gillet, E. *Surf. Sci.* **1990**, *238*, 75−82.
(54) Ruff, M.; Takehiro, N.; Liu, P.; Nørskov, J. K.; Behm, R. J. *ChemPhysChem* **2007**, *8*, 2068−2071.
(55) Liu, P.; Nørskov, J. K. *Phys. Chem. Chem. Phys.* **2001**, *3*, 3814−3818.
(56) Rozmysłowicz, B.; Mäki-Arvela, P.; Tokarev, A.; Leino, A. R.; Eränen, K.; Murzin, D. Y. *Ind. Eng. Chem. Res.* **2012**, *51*, 8922−8927.
(57) Bartholomew, C. H.; Farrauto, R. J. *Fundamentals of industrial catalytic processes*; Wiley: New York, 2011.
(58) Lamb, H. H.; Sremaniak, L.; Whitten, J. L. *Surf. Sci.* **2012**, *607*, 130−137.
(59) Lu, J.; Behtash, S.; Heyden, A. *J. Phys. Chem. C* **2012**, *116*, 14328−14341.
(60) Wilson, A. R.; Sun, K.; Chi, M.; White, R. M.; LeBeau, J. M.; Lamb, H. H.; Wiley, B. J. *J. Phys. Chem. C* **2013**, *117*, 17557−17566.
(61) Ping, E. W.; Pierson, J.; Wallace, R.; Miller, J. T.; Fuller, T. F.; Jones, C. W. *Appl. Catal., A* **2011**, *396*, 85−90.
(62) Mallard, W.; Linstrom, P. *NIST Standard Reference Database* 2000, *69*.




DOI: 10.1021/cs501865n
*ACS Catal.* 2015, 5, 1939−1948